frontiers | Frontiers in Built Environment

TYPE Original Research
PUBLISHED 28 November 2024
DOI 10.3389/fbuil.2024.1468703

OPEN ACCESS

EDITED BY
Yongliang Liu,
Jilin University, China

REVIEWED BY
Michał Łach,
Cracow University of Technology, Poland
Sergiu-Mihai Alexa-Stratulat,
Gheorghe Asachi Technical University of Iași, Romania

*CORRESPONDENCE
Thandiwe Sithole,
nastassias@uj.ac.za

RECEIVED 22 July 2024
ACCEPTED 14 November 2024
PUBLISHED 28 November 2024

CITATION
Nseke J, Kirkelund GM and Sithole T (2024) The inhibitory influence of rice husk ash on the alkali leaching and efflorescence extents of alkali activated granulated blast furnace slag.
Front. Built Environ. 10:1468703.
doi: 10.3389/fbuil.2024.1468703

The inhibitory influence of rice husk ash on the alkali leaching and efflorescence extents of alkali activated granulated blast furnace slag

Joseph Nseke[1], Gunvor Marie Kirkelund[2,3] and Thandiwe Sithole[1]*

[1]Department of Chemical Engineering, University of Johannesburg, Johannesburg, South Africa, [2]Department of Civil Engineering, Technical University of Denmark, Kongens Lyngby, Denmark, [3]School of Chemistry, Shoolini University, Solan, India

This study investigates the inhibitory effect of rice husk ash (RHA) on the efflorescence and leaching of alkali-activated granulated blast furnace slag (GBFS). RHA consists of about 90% of microporous amorphous silica and possesses similar pozzolanic characteristics to silica fume and nano-SiO_2. The specific surface area of RHA varies between 20 and 200 m^2/g. RHA-GBFS-based specimens were mainly characterised through Fourier transform infrared spectroscopic (FTIR), X-ray diffraction spectrometry (XRD), thermal analyses, as well as scanning electron microscope (SEM) and energy dispersive spectrometric (EDS) analyses. Results showed that efflorescence decreases with the rise in RHA content due to the increase in the degree of reaction. The optimal RHA content was 15%. Specimen consisting of 15% RHA and 85% GBFS yielded the lowest extent of total alkali leaching, equivalent to 9.41%, while sample consisting of 100% GBFS yielded the highest degree of alkali leaching, equivalent to 29.9%. EDS analysis of 15% of specimens before and after leaching indicates a smaller decrease in Na^+ ions from 27.83% to 25.25% by weight. However, the addition of RHA does not permanently inhibit alkali leaching but retard the extent of alkali leaching over time. With the increase of up to 15% RHA, CO^{3-} peaks are nearly suppressed based on FTIR analysis, indicating that the increase in RHA mitigates the effect of efflorescence. XRD of specimens containing 10% and 15% RHA \ indicate the possible formation of hydrosodalite and sodium-calcium aluminium hydrate gel, which control the mobility of Na + ions; consequently, Na + ions are less prone to reach out.

KEYWORDS

rice husk ash, granulated blast furnace slag, efflorescence, alkali leaching, alkali activated material

1 Introduction

Alkali-activated materials (AAMs) are versatile and forward-looking materials that inherently possess good physical, mechanical, and cementing properties that are

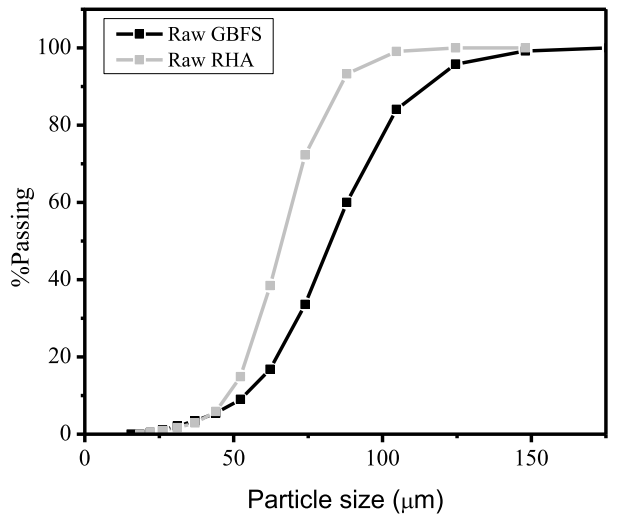

FIGURE 1
Particle size distribution of GBFS and RHA.

advantageous for building and construction applications (Wang et al., 2020). As constituents of a wide range of precursors, slags have been extensively used to develop AAMS due to the emergent incentive to promote the circular economy by upcycling slags and preserving the natural environment (Nodehi and Taghvaee, 2022). Extensive research has been carried out mainly on the alkali-activation of granulated blast slags (GBFS) (Manjunath and Narasimhan, 2020; Criado et al., 2017). The quantity of world-widely generated GBFS has varied between 2.1 and 6.4 billion tons for 12 years starting from 2005 (Kambole et al., 2019). Over the same elapsed period, the South African iron-making industry has generated about 12 and 37 million tons of GBFS (Edwards, 2014). Succinctly, principal environmental issues originating from the global generation of GBFS are associated with the expansion of the land area for the disposal of slags, potential pollution of the anthroposphere and loss of biodiversity over time (Kambole et al., 2019). Hence, these issues call upon the need to re-use and recycle globally generated slags to minimize potential adverse environmental impacts (Kambole et al., 2019). One reliable and cost-effective alternative can be based on developing AAMs using GBFS as a precursor.

Although alkali-activated GBFS-based materials are reported to exhibit good physical and mechanical properties based on their strength and volumetric stability due to insignificant content or the lack of free lime (f-CaO) in GBFS, despite all the benefits mentioned above offered by the development of alkali-activated materials, AAMs are subjected to a problem of efflorescence, sub-fluorescence and alkali leaching (Longhi et al., 2019; Zhang et al., 2018; Allahverdi et al., 2015; Saludung et al., 2021). The occurrence of efflorescence and sub-fluorescence is a function of different factors, such as the material properties, exposition, and the surrounding effects. Efflorescence and sub-fluorescence are both associated with the carbonation process (Zhang et al., 2018). However, efflorescence occurs when internal alkalis are displaced toward the surface of AAMs, supplying alkali ions for the precipitation of carbonate salts in the presence of dissolved CO_2 under equilibrium conditions between the pore solution and the crystal (Zhang et al., 2018; Škvára et al., 2009).

Considering that AAMs are microporous materials, the transport of internal alkalis-containing solutions toward the surface is carried out by capillary pressure, which depends on the pore size distribution. On the drying surface, as the salts containing solution evaporate, the concentration of the dissolved salts rises; precipitation of salts thus becomes feasible at a high supersaturated level (Scherer, 2004). Conversely, sub-fluorescence is related to the internal crystallization of carbonate salts within pores in a depth sufficient to promote absorption of dissolved CO_2. In essence, sub-fluorescence occurs below the evaporation region. In the case of AAMs, internal crystallization of salts takes place when the relative air humidity RH is below the equilibrium salt humidity Hr_{eq} ($RH < Hr_{eq}$) (Longhi et al., 2019). Na_2CO_3 Hr_{eq} at 20°C is equivalent to 91.6% (Apelblat and Manzurola, 2003).

Equations 1, 2 represent the overall spontaneous reactions involved in forming salt precipitates on the surface of alkali-activated materials in Eqn. The formation of carbonate hydrates is given in Equation 3.

$$NaOH\,(aq) + CO_2 \rightarrow Na_2CO_3\,(s) + H_2O\,(\Delta G^o = -128.97KJ/mol) \quad (1)$$

$$NaOH\,(aq) + CO_2 \rightarrow NaHCO_3\,(s)\,(\Delta G^o = -29.56KJ/mol) \quad (2)$$

$$Na_2CO_3 + xH_2O \rightarrow NaCO_3.xH_2O \quad (3)$$

On the surface, the initial effect of efflorescence is related to aesthetical defects with no significant impact on the structural integrity of the materials (Longhi et al., 2019). However, continually uncontrolled sub-fluorescence can internally develop and create vulnerable regions within the material leading to spalling due to the rise in internal stresses induced by the pressure from crystallized efflorescence product and through freeze-thaw cycling over time (Allahverdi et al., 2015). Several studies have been carried out with the aim focused on investigating and developing methods to control the efflorescence of alkali materials and the extent of alkali leaching (Wang et al., 2020; Longhi et al., 2019; Saludung et al., 2021; Škvára et al., 2009; Kani et al., 2012; Zhang et al., 2014; Srinivasamurthy et al., 2021; Zhu et al., 2022).

According to Škvára et al. (2009), using a high curing temperature range to produce AAMs has been reported to have reduced the efflorescence extent due to enhancing the degree of alkaline reaction. Kani et al. (2012) investigated the effect of the addition of calcium aluminate cement (CAC) on alkali-activated pumice-type natural pozzolanic materials. They stipulated that during the synthesis of AAMs, Si-O-Al polymeric network becomes negatively charged as the content of aluminium increases. Consequently, alkalis would generally form strong bonds with the negatively Si-O-Al network through electrostatic forces and produce a stable neutrally charged compound structure similar to zeolites in the later polymerization stage.

Na^+ ions from zeolites are stabilized and are ascertained to be highly insoluble in water. As a result, a decrease in AAMs' alkali leaching and efflorescence extent could be observed. However,

TABLE 1 Chemical composition of raw materials.

Composition (wt%)											
	Al_2O_3	CaO	Fe_2O_3	K_2O	MgO	Na_2O	P_2O_5	SiO_2	SO_3	Others	LOI
GBFS	10.27	33.66	0.60	0.91	5.51	16.74	0.00	27.02	1.65	2.23	1.41
RHA	0.24	2.28	0.26	7.43	0.43	0.03	1.13	87.17	0.43	0.44	0.16

TABLE 2 Experimental design.

GBFS (mass%)	RHA (mass%)	Temperature (°C)	Curing period (days)	L/S
100	0	80	1 + 4	0.4
95	5	80	1 + 4	0.4
90	10	80	1 + 4	0.4
85	15	80	1 + 4	0.4

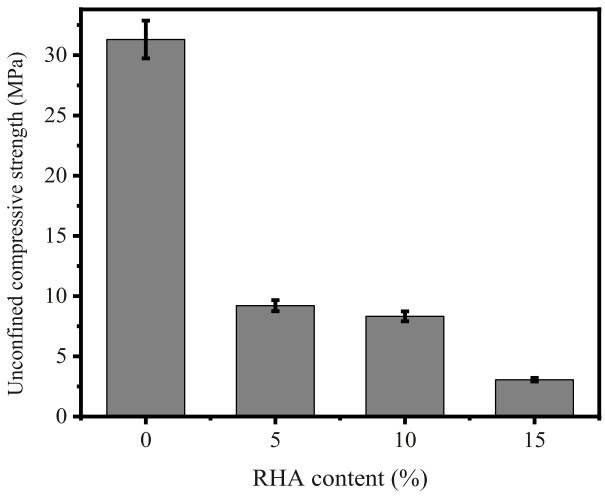

FIGURE 2
Mechanical characteristics of synthesized specimens.

sources of reactive alumina, such as calcium aluminate cement, can be considerably costly (Hewlett and Liska, 2012). Zhang et al. (2014) reported that the replacement of fly ash with the slag up to 20 per cent had a less considerable effect on efflorescence, as it only had the tendency of retarding rather than attenuating the development of efflorescence. Results from a previous study by Lach et al. (2020) however indicate that hydrothermally treated geopolymers with TiO_2 and aluminum calcium cement additives were significantly less susceptible to efflorescence. Lach et al. (2020) stipulate that during hydrothermal treatment, the excess Na^+ ions are flushed out, making the geopolymers less prone to efflorescence.

With the same perspective, the current study evaluates the influence of adding rice husk ash (RHA) on the extent of efflorescence and alkali leaching of alkali-activated GBFS-based specimens. RHA is a readily available material produced from direct incineration of the rice husk. To date, 700 million tons of rice husk have been produced (Singh, 2018). RHA can also be obtained as a by-product of gasification of rice husk from which a renewable source of green energy referred to as syngas is generated (Shen et al., 2014; Yoon et al., 2012). Sub-Saharan African rice hush ash production is reported to be ± 20 million. In a previous study, ordinary Portland cement replacement with of rice husk ash up to 30% by volume yielded high compressive strength (Msinjili and Schmidt, 2014). However, unlike previous studies that only examined the effect of RHA on the compressive strength of geopolymers, the novelty of the current study lies in its exploration of the underlying mechanism by which RHA has the potential to inhibit efflorescence.

RHA consists of about 90% of amorphous silica and possesses similar pozzolanic characteristics with high microporosity compared to other sources of reactive silica such as silica fume and nano-SiO_2. Results from Brunauer–Emmett–Teller (BET) nitrogen adsorption analysis revealed that the specific surface area of RHA could vary between 20 and 200 m^2/g while that of silica fume ranged from 18 to 23 m^2/g (Singh, 2018). Saludung et al. (2021) reported that silica fume (SF) had reduced the extent of efflorescence and alkali leaching due to the increase in the degree of reaction and the decrease in Na/Si atomic ratio leading to immobility of alkalis. Moreover, Zhu et al. (2022) reported that silica fume -GBFS-based materials consisted of calcium silicate hydrate and zeolitic phases; however, the leaching extent had not been significantly altered for aged AAMs.

This study aimed to investigate the feasibility of mitigating the efflorescence and alkali leaching impact on AAMs using RHA, thus providing insight and adding to the existing literature on the effect of RHA on the extent of efflorescence and alkali leaching of alkali-activated GBFS based AAMs.

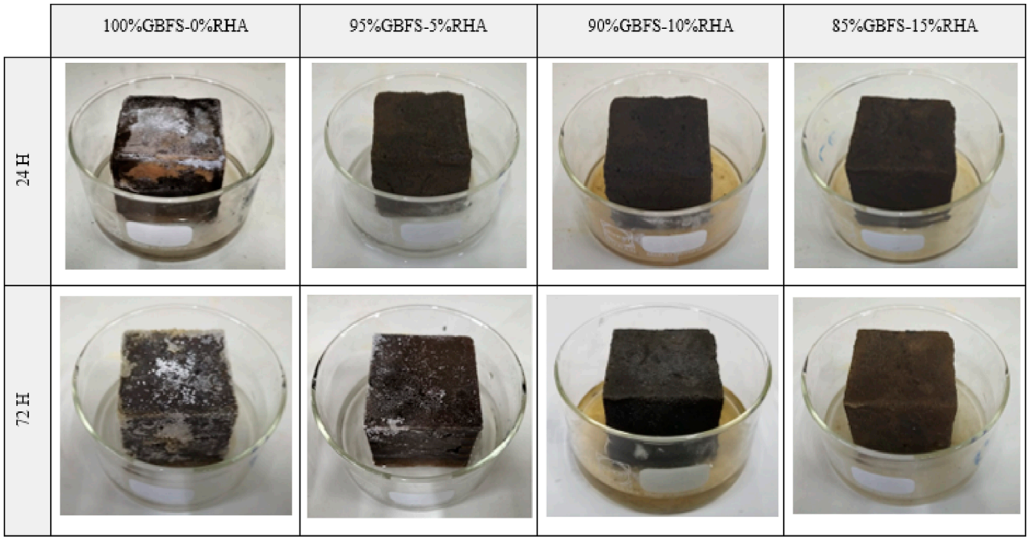

FIGURE 3
Efflorescence evaluation after 24 and 72 h.

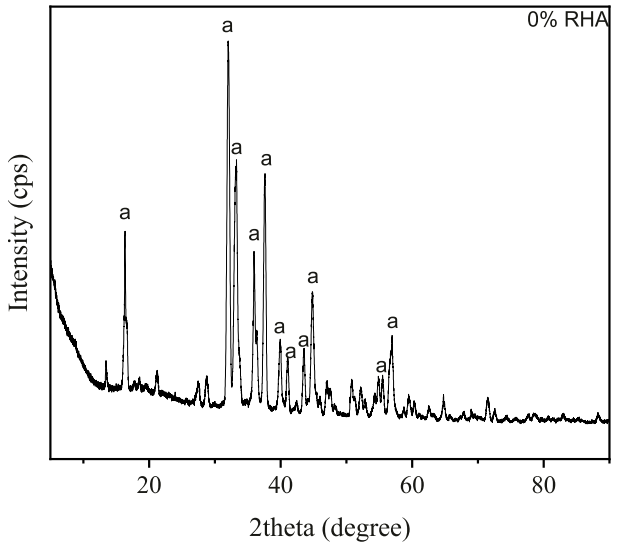

FIGURE 4
X-ray diffractogram of the efflorescence product. a: Thermonatrite ($Na_2CO_3.H_2O$).

2 Materials and methods

2.1 Materials

GBFS and RHA were used as raw materials to synthesize alkali-activated specimens. ArcelorMittal supplied GBFS, and RHA was obtained through controlled combustion of rice husk at 600°C for 1 h in an ash furnace. According to Singh (2018), the burning temperature under controlled rice husk combustion varies from 500 to 700°C to obtain the reactive amorphous silica. 99% pure sodium hydroxide purchased from Sigma Aldrich was used as the sole alkali activator. The raw materials were calcined at 1000°C for 3 h to determine the percentage of loss on ignition (LOI) (Sithole and Mareya, 2023). The particle size distribution and chemical composition of the raw materials are presented in Figure 1 and Table 1 respectively. The raw materials consist of particles with more than 80% passing through a 100 µm sieve.

2.2 Method

2.2.1 Synthesis of alkali activated specimen

Synthesis of alkali-activated specimen consisted of mechanically mixing a solution of 15 M NaOH with a blend of GBFS and RHA solids for 2 min using a mechanical mixer at a constant liquid to solid (L/s) equivalent to 0.4 (Azad and Samarakoon, 2021). BFS particle size was reduced to −100 µm before synthesis to enhance the degree of reaction. RHA mass% content in the blend varied from 0% to 15%, producing 3 samples for each mix design. Further increase in RHA is associated with low workability (Bayraktar and Fello, 2023). The homogeneously mixed paste was cast into 50 × 50 × 50 mm^3 cubic moulds and kept for 24 h to consolidate at ambient temperature. Subsequently, the consolidated specimens were de-moulded and placed in the oven at 80°C for 4 days to ensure the completion of the reaction. High curing temperature accelerates the hydration process of precursors (Shi et al., 2023). The moulds containing the AAM specimen were sealed with a steal board so as to minimize loss of moisture or capillary water, which enhances drying shrinkage and cracks (Mo et al., 2014). Lastly, synthesized specimens were sealed in polyethene bags to inhibit carbonation and prevent a decrease in alkalinity. Table 2 summarizes the parameters of the mixing design used in the study.

The mechanical characteristics measured using Matest compression test Machine of synthesized specimens with varied RHA content are presented in Figure 2, whereby it is observed that higher content decreases the strength of materials.

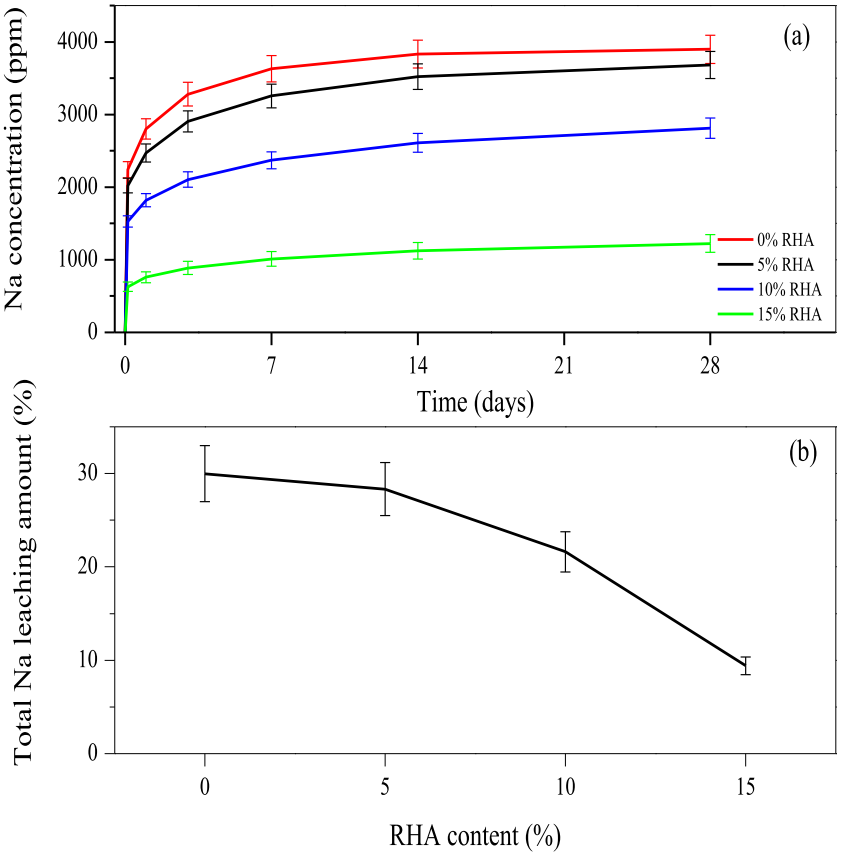

FIGURE 5
The effect of RHA content on alkali leaching. **(A)** Na concentration (ppm) as a function of time; **(B)** Total Na leaching amount % as function of RHA content.

TABLE 3 Energy dispersive spectrometric analysis of specimens.

RHA content	Initial composition				Final composition after 28 days			
	0%	5%	10%	15%	0%	5%	10%	15%
Na	25.66	26.82	26.68	27.83	16.91	19.84	21.09	25.25
Mg	2.31	2.66	2.53	2.53	2.59	2.45	2.44	2.58
Al	4.02	4.13	4.05	3.82	4.01	3.93	3.71	3.77
Si	12.77	13.53	14.35	14.95	11.97	14.02	12.6	13.06
S	0.82	0.71	0.67	0.69	0.69	0.65	0.67	0.69
K	0.71	0.98	1.24	1.11	0.93	1.17	1.09	0.89
Ca	16.32	12.3	11.51	10.29	11.95	11.17	9.99	11.71
Ti	0.34	0.36	0.31	-	0.35	0.3	0.3	0.04
Mn	1.15	1.5	1.32	1.26	1.46	1.28	1.21	1.43
Fe	0.32	—	—	—	0.22	—	—	—
O	35.58	37.02	37.34	37.52	48.92	45.19	46.9	40.58

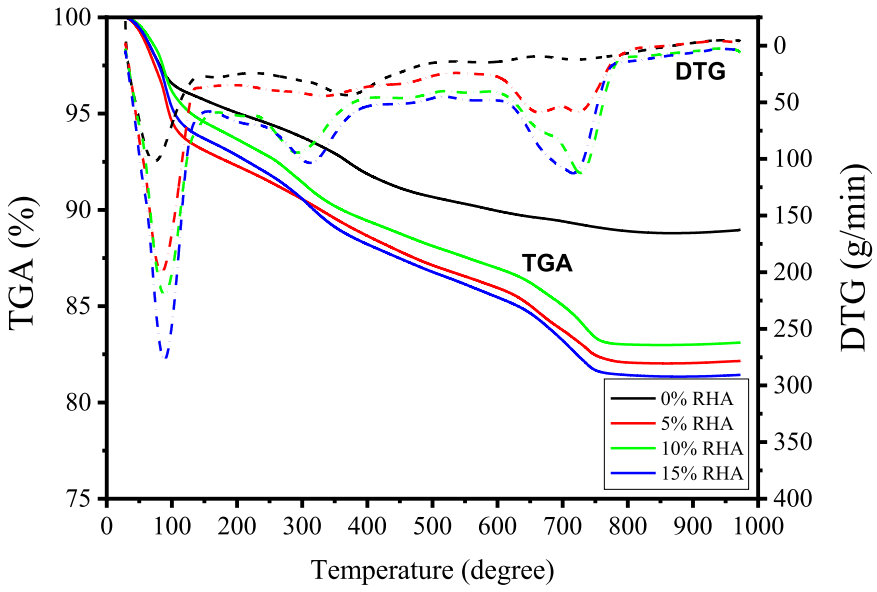

FIGURE 6
Thermal analysis of alkali-activated GBFS-RHA based specimens at various contents.

TABLE 4 TG-DTG data of alkali-activated GBFS-RHA based specimens.

RHA content	Temperature (°C)	Mass loss % after evaporation of free water	Phase transformation	Residual mass% above 800°C
0% RHA	98	5	590	88
5%RHA	98	5	650	83
10% RHA	98	5	650	83
15%RHA	98	6	650	81

TABLE 5 DTA Analysis of specimens.

Temperature (degree)	Phase change	Reaction
98	Free water evaporation	Endothermic
748	Phase transformation of C-SH to Wollastonite	Exothermic

2.2.2 Alkali leaching and efflorescence experiment

Static alkali leaching experiments were conducted to investigate RHA content's effect on the extent of alkali leaching. First, synthesized specimens with various RHA content were comminuted and screened. The solid feed consisted of a fraction of alkali-activated GBFS-RHA fragments with particle sizes varying from 2.36 to 4.75 mm (Saludung et al., 2021). Solid to liquid was equivalent to 1:20. Aliquots from leaching vessels were collected after 3 h, 24 h, 72 h, 7 days, 14 days and 28 days. There were two replicates for each mix design. Visual and direct observation were primarily used to observe efflorescence on the specimen. Specimens were placed in open Pyrex glasses which were partially filled with 5 mL of deionized water. The water level was adjusted up to 5 mm for all the efflorescence tests. Efflorescence images were captured after 24 h and 72 h. After 72 h, the change in the observed efflorescence was relatively insignificant.

2.2.3 Water absorption

Determination of water absorption capacity and porosity of specimens was carried out by soaking the dried specimen at 20°C for 24 h according to ASTM C62 standard. Before submersion,

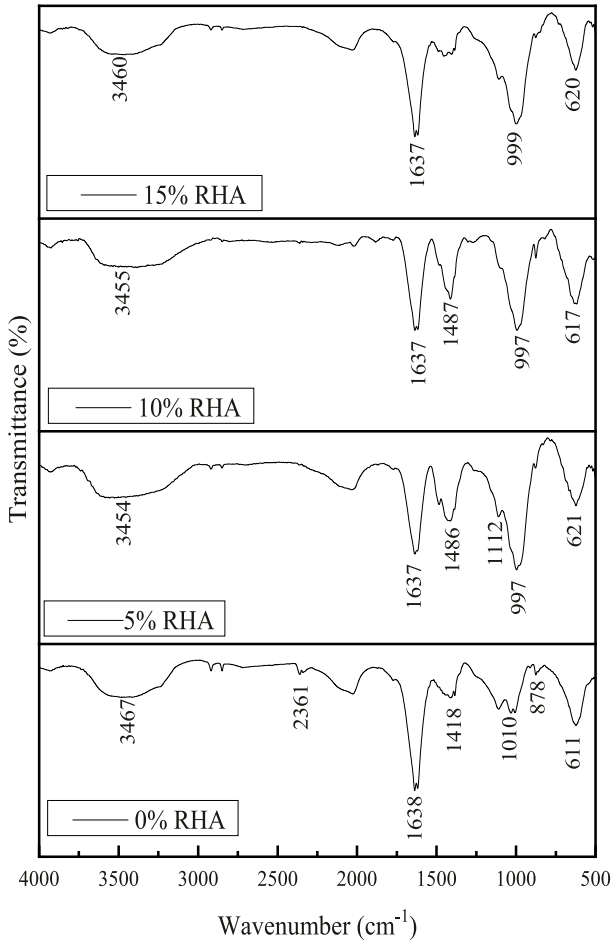

FIGURE 7
FTIR spectrum of GBFS-RHA based specimen at varied RHA content.

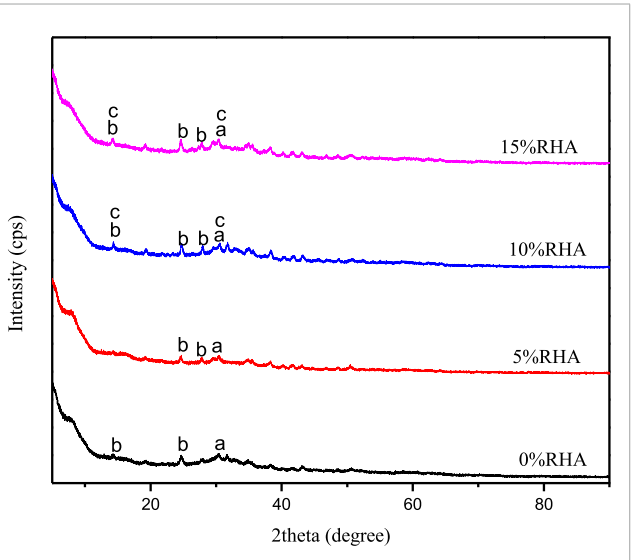

FIGURE 8
X-ray diffractogram of alkali activated GBFS specimen with varied RHA content. **(A)** Calcium silicate hydrate (C-S-H), **(B)** Hydrosodalite, **(C)** Sodium Calcium aluminium silicate hydrate (C-N-A-S-H).

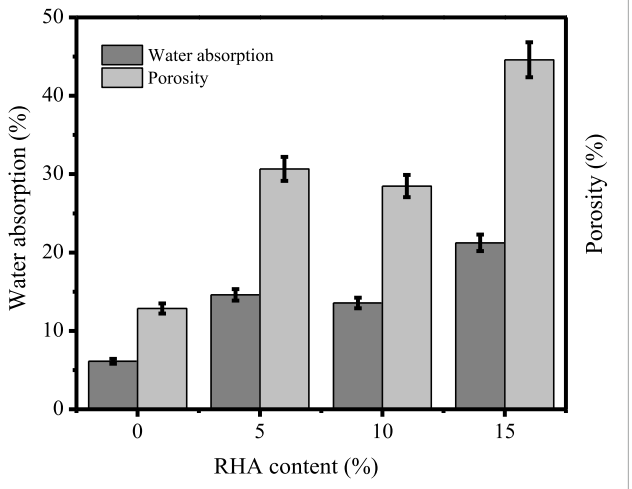

FIGURE 9
Water absorption capacity and macro-porosity of specimens.

synthesized cubic specimens were dried at 80°C until no fluctuation in the weight of dried specimens was observed. Each reported water absorption capacity is the mean value of 3 specimens synthesized under the same condition. Water absorption capacity % (W_{AC}%) is calculated according to Equation 4 whereby m_i and m_f are the masses of the specimen before and after, immersion respectively.

$$W_A(\%) = 100 \times \frac{m_{f-}m_i}{m_i} \quad (4)$$

2.2.4 Characterization

Characterization of synthesized specimens (in a powder form) was carried out through x-ray fluorescence (XRF), x-ray diffraction (XRD), scanning electron microscope-energy dispersive spectrometry (SEM-EDS), Fourier transforms infrared spectroscopic (FTIR) and thermal analyses. Chemical compositions of raw materials were analyzed using an automatically calibrated Rigaku model Primus IV spectrometer operating at 40 mA and 50 V. For mineralogical analysis, specimens were scanned at 0.5°C/min from 5° to 90° (2 theta) with a Rigaku model Ultima IV XRD spectrometer using a copper K*x-ray source, operating at 30 mA and 40 V and equipped with a PXDL software program. An EDS Vega 3 SEM with a high voltage setting and beam intensity of 20 V and 11 W/cm2 was used to determine carbon-coated specimens' morphology, microstructure, and elemental composition. The study of chemical bonds within the specimen was carried out using a Thermofisher FTIR spectroscope. Specimen were scanned from 400 to 4,000 cm^{-1} with resolution set at 4 cm^{-1} and the number of scans equivalent to 32 scans. A thermal decomposition study based on thermal gravimetric (TGA) and differential thermal analyses (DTA) was carried out from room temperature to 950°C with a heating rate of 20°C/min. The surface area and micropore volume of the samples from different specimens were determined using a BET surface analyser Tri Star II Plus 3. Before analysis, the samples were degassed at 100°C for 6 h. N_2 at 80.2 K was used for adsorption-desorption tests.

TABLE 6 BET analysis.

	Micropore Volume (cm^3/g)	Micropore diameter (nm)	Cross-sectional Area (nm^2)	BET surface Area (m^2/g)
0% RHA	0.422	20.611	0.125	0.550
5% RHA	0.665	25.962	0.125	0.740
10% RHA	0.735	30.55	0.125	0.811
15% RHA	0.995	53.55	0.125	1.05

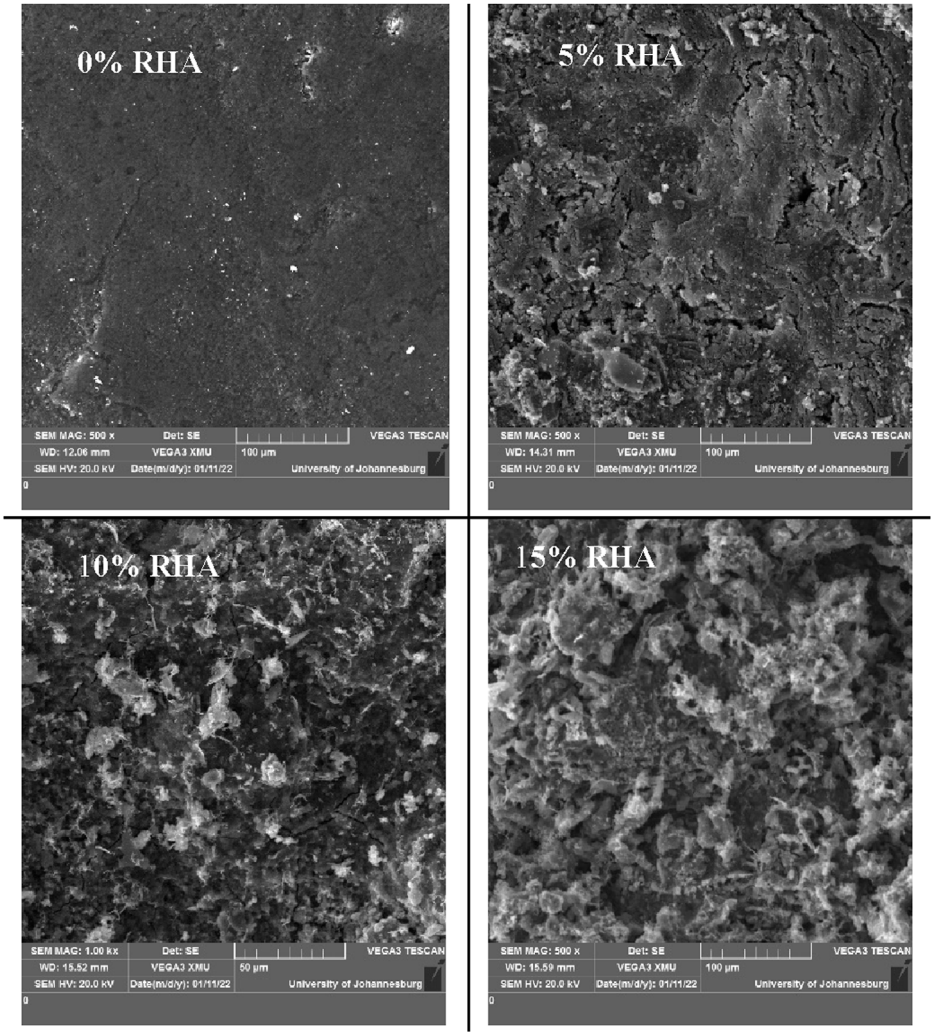

FIGURE 10
SEM micrographs of the specimens.

3 Results and discussion

3.1 Effect of RHA on efflorescence and alkali leaching

3.1.1 Efflorescence

Figure 3 shows the efflorescence evaluation after a period of 24 and 72 h. The results primarily based on direct visual observation of alkali activated GBFS based specimens synthesized with and without RHA additives. It has been demonstrated that the extent of efflorescence decreases with the rise in RHA content. Observed efflorescence on 100% GBFS - 0% RHA specimen after 24 and 72 h is caused by the excess of unreacted sodium hydroxide, thus able to migrate from the pore solutions to the surface and subsequently react with dissolved atmospheric carbon dioxide to generate carbonate salts in the form of $NaHCO_3$. xH_2O and

Na_2CO_3. xH_2O. The x-ray diffractogram of salt deposited on 100% GBFS-0% RHA specimen after 72 h is shown in Figure 4, whereby the high predominance of a sodium carbonate monohydrate polymorph referred to as thermonatrite (DB number: 01-076-0910) has been observed. As aforementioned, efflorescence is associated with the unaesthetic appearance of the alkali-activated material with no direct detrimental impact on the integrity of AAM. Nevertheless, efflorescence can be exacerbated by high moisture content drawbacks leading to the spalling of the manufactured AAM. However, as RHA content increases, the efflorescence can be retarded or hindered over time, as observed in the current study.

Previous studies by Sun et al. (2020) and Saludung et al. (2021) plainly explain the underlying mechanism through which a highly reactive silica exhibit its inhibitory influence on the efflorescence of alkali-activated materials. The underlying mechanism lies in the fact that reactive silica increases the degree of reaction through which a gel is possibly formed and subsequently fills the pore solution within the matrix of the AAMs. With the addition of reactive silica, the Na + diffusion rate from the pore solution to the AAMs surface decreases to some extent (Liaudat et al., 2020).

In conjunction with previous studies, the analogy between the intrinsic properties of RHA and those of previously studied sources of highly reactive silica can be established. The specific area of RHA varies between 20 and 200 m^2/g whilst the range of the particular area of silica fume is from 18 to 23 m^2/g, and that of nano-SiO_2 has been reported to be 296 m^2/g. Consequently, amorphous silica from RHA is as reactive as the SF and nano-SiO_2. Moreover, it can also be inferred that the aforementioned underlying mechanism through which the decrease of the extent of efflorescence is achieved correlates with the inhibitory influence of RHA on the efflorescence formation on the surface of synthesized specimens in the current study.

3.1.2 Alkali leaching

The effect of RHA content on the alkali leaching extent is illustrated in Figures 5A, B. Figure 5A indicates that the extent of alkali leaching initially rises and remains relatively constant over time. Without the addition of RHA, Na^+ ions concentration in the eluate is high due to the excess of unreacted Na^+ ions in the form of $Na(H_2O)_n^+$ or hydroxyl ions in the pore solution within the synthesized specimen. These alkali hydroxyl ions form weaker bonds with the pore solution than alkali Na^+ ions (Sun et al., 2020). Consequently, alkali hydroxyl ions weakly bound to the calcium aluminosilicates are readily subjected to hydrolysis and increase the concentration of Na^+ ion concentration of the eluate. Conversely, with the addition of RHA, it is observed that the Na^+ concentrations of each specimen in water drop with the increase in the RHA content in the alkali-activated GBFS-based specimen over the immersion period of 28 days. However, the addition of RHA does not permanently inhibit alkali leaching but rather retard the extent of alkali leaching over time. In Figure 5B, results demonstrate that the addition of RHA leads to a significant decrease in the extent of total alkali leaching from 29.9% to 9.41%. In other words, the alkali leaching extent has been reduced by 69.56% with the addition of 15% mass of RHA.

In Table 3, the dispersive energy analysis ascertains an increase of up to 15% RHA stabilizes Na^+ ions from leaching away in contact with water. Hence, 15% RHA (mass%) was the optimum. Compared to the previous study by (Saludung et al., 2021), the observed drop in the alkali leaching extent with the silica addition of silica fume (SF) has been reported from about 67% to 56%. The decrease in alkali leaching is due to the Na/Si ratio (Saludung et al., 2021) which increases with the increase in silica content. Additionally, in the current study, it could be stipulated that forming a gel-like structure able to stabilize Na^+ ions is favored with the addition of RHA that contains reactive amorphous silica and increases the reaction rate. Moreover, at high, pH, reactive silica from RHA and aluminum ions reacts with OH- to form Si-O-Si and Al-O-Al. Subsequently substitution of Si^{4+} with Al^{3+} is more prominent as results of similarity in atomic size, leading to a negative charge imbalance in the crystal lattice. In the later stage, the negative charge imbalance is neutralized by the alkalis. The bonds alkalis between the Si-O-Al structure are characterized by a strong electrostatic force. Consequently, the transport properties of Na^+ ions are altered so that fewer Na^+ ions migrate to the water.

3.2 Thermal analysis

Thermal analysis plots are shown in Figure 6. The mass loss at 98°C is due to the evaporation of the free water within the pore solutions of the specimens. From 200°C to 600°C, removal of chemically bound water from the calcium silicate hydrate further mass loss of the total mass of the specimens. The peak at 300°C for DTG of 10% and 15% RHA samples is associated with the carbonization which is highly influenced by the content of Si. The peak is not well defined at low content of RHA due to the limited amount of Si (Ramadhansyah et al., 2012). At 800°C, C-S-H is completely transformed to wollastonite ($CaSiO_3$). From 200°C, it can be observed that the total mass loss of specimens rises with the increase in RHA due to the dehydration of hydrates. TG-DTG data of alkali-activated GBFS-RHA based specimens are provided in Table 4. Considering that the content of chemically bound water to hydrates is directly proportional to the content of formed hydrates, it could be inferred that the addition of RHA enhances the degree of reaction. Consequently, the amount of unreacted sodium hydroxide is expected to decrease and ensures that the efflorescence extent is controlled or completely inhibited, as observed in Figure 3. In Table 5, DTA parameters are presented. Two major temperature points are observed at 98°C and 748°C. The first and second points are associated with the endothermic evaporation of free water within the pore solution and the exothermic phase transformation oFf C-S-H to wollastonite.

3.3 FTIR analysis

Chemical bonds within the alkali-activated GBFS-RHA based materials indubitably play an essential role in the alkali-leaching and

the efflorescence extent. FTIR analysis of specimen at varied RHA contents in Figure 7 mainly indicates the presence of calcium silicate hydrate with aluminum substituting silicon and leading to the formation of calcium aluminium silicate hydrate, which is revealed at lower wavenumber ranging from 500 to 1,200 cm^{-1} (Sun et al., 2020). Broadband between 2,600 cm^{-1} and 3650 cm^{-1} indicates O-H stretching vibration emanating from hydration products. The shift from 1100 cm^{-1} to lower wavenumber (999 and 997 cm^{-1}) possibly indicates an increase in the extent of reaction with an increase in RHA content which possibly leads to the mitigation of the efflorescence effect.

Ideally, with Al substitution for Si, the Si-O-T network structure becomes negatively charged, and alkalis within the pore solution are bound to the structure by Coulomb forces leading to the decrease more than free Na^+ ions, which are readily leached out from the specimen to the water. Hence, inhibitory influence on the alkali leaching extent of the specimen could be possibly observed. Frequency bands from 1,400 cm^{-1} to 1,600 cm^{-1} can be assigned to the CO_3^{2-}asymmetric vibrations. At 15%RHA, CO^{3-} peaks at 878 cm^{-1} are nearly suppressed, indicating that the increase in RHA mitigates the effect of efflorescence.

3.4 X-ray diffraction analysis

Results from x-ray diffraction analysis of synthesized specimens at varied RHA content in Figure 8 showed an amorphous structure for all the synthesized specimen associated with the development of poorly crystalline phases as the RHA content increases. The result of poorly crystalline phases possibly stipulates that the inclusion of RHA in the synthesis of activated GBFS based specimens enhances the degree of reaction. The concentration of free alkalis within the pore solutions decreases with the rise in the degree of reaction (Lindgård et al., 2012). Hence, it could be observed that the extent of the efflorescence reduced with the inclusion of RHA up to 15%.

The poorly crystalline phase mainly consists of calcium silicate hydrate in all the specimens. X-ray diffractogram of specimen containing 10% and 15% RHA additionally indicates the possible formation of hydrosodalite and sodium-calcium aluminium hydrate gel, which control the mobility of Na^+ ions; consequently, Na^+ ions are less prone to leach out. Na^+ ions are held by electrostatic forces forming strong bonds within the structure of hydrosodalite and sodium-calcium aluminate hydrate gel depending on the Ca/Al and Si/Al ratios. Moreover, the transport properties of alkalis from the pore solution to the surface are altered with gel formation.

3.5 Water absorption and porosity

Evaluation of physical characteristics of specimens based on the water absorption and porosity is a salient aspect to be considered in the manufacturing of construction materials. In Figure 9, the effect of the addition of RHA on the water absorption and porosity per cent of the specimens is evaluated. It has been observed that the macro-porosity and water absorption (vol%) respectively rise from 14.2% to 40% (v/v) with the increase of RHA and from 6.1% to 21.9% (w/w). However, previous results by Saludung et al. (2021) indicate the lowest water absorption for 0%RHA specimen to be equivalent to 3.51%.

Similar trends were observed based on the BET analysis. The results in Table 6 indicate an increase in micropore volume of nearly 136% with the increase in RHA content from 0% to 15%. Additionally, in Figure 10, micrographs of specimen at different RHA contents show the development of rough surface with pores as the RHA content increases, possibly leading to the increase in water absorption at high RHA content. Based on the water absorption and porosity results, an RHA content increase of up to 10% can be regarded as the optimal condition.

4 Conclusion

This study focused on evaluating the feasibility of inhibiting the efflorescence formation and monitoring alkali-leaching extent with the addition of rice husk ash for the development of alkali-activated GBFS based materials. RHA is a highly available and inexpensive material which consists of about 90% of amorphous silica. It possesses similar pozzolanic characteristics with high microporosity when compared to other sources of reactive silica such as silica fume and nano-SiO_2.

- It has been demonstrated that the extent of efflorescence decreases with the rise in RHA content. At 15% RHA, CO^{3-} peaks are nearly suppressed based on FTIR analysis, which may indicate that the increase in RHA mitigates the effect of efflorescence.
- Considering that the content of chemically bound water to hydrates is directly proportional to the content of formed hydrates, it could be inferred that the addition of RHA enhances the degree of reaction.
- X-ray diffractogram of specimen containing 10% and 15% RHA indicates the possible formation of hydrosodalite and sodium-calcium aluminium hydrate gel, which control the mobility of Na^+ ions; consequently, Na^+ ions are less prone to leach out. Na^+ ion concentration leaching decreased from 29.9 to 9.4 with the increase of RHA content up to 15%. However, the addition of RHA does not permanently inhibit alkali leaching but rather retard the extent of alkali leaching over time.

Data availability statement

The original contributions presented in the study are included in the article/supplementary material, further inquiries can be directed to the corresponding author.

Author contributions

JN: Data curation, Formal Analysis, Investigation, Methodology, Writing–original draft. GK: Visualization, Writing–review and editing. TS: Conceptualization, Funding acquisition, Investigation, Methodology, Resources, Supervision, Validation, Writing–original draft.

Funding

The author(s) declare that financial support was received for the research, authorship, and/or publication of this article. The authors wish to thank the University of Johannesburg (URC) grant number: 2021URC00287 and National Research Foundation (ZA), Grant Unique Number: BAAP200512521382.

Conflict of interest

The authors declare that the research was conducted in the absence of any commercial or financial relationships that could be construed as a potential conflict of interest.

Publisher's note

References

Allahverdi, A., Kani, E. N., Hossain, K. M. A., and Lachemi, M. (2015). "Methods to control efflorescence in alkali-activated cement-based materials," in *Handbook of alkali-activated cements, mortars and concretes* (Cambridge, United Kingdom: Woodhead Publishing), 463–483.

Apelblat, A., and Manzurola, E. (2003). Solubilities and vapour pressures of saturated aqueous solutions of sodium tetraborate, sodium carbonate, and magnesium sulfate and freezing-temperature lowerings of sodium tetraborate and sodium carbonate solutions. *J. Chem. Thermodyn.* 35 (2), 221–238. doi:10.1016/s0021-9614(02)00308-7

Azad, N. M., and Samarakoon, S. S. M. (2021). Utilization of industrial by-products/waste to manufacture geopolymer cement/concrete. *Sustainability* 13 (2), 873. doi:10.3390/su13020873

Bayraktar, O. Y., and Fello, F. M. A. (2023). The effect of RHA and GBFS on the mechanical and physical properties of cementitious composites with high early age compressive and flexural strength: bayesian algorithm for the design. *Iran. J. Sci. Technol. Trans. Civ. Eng.* 48, 97–115. doi:10.1007/s40996-023-01168-w

Criado, M., Ke, X., Provis, J. L., and Bernal, S. A. (2017). "Alternative inorganic binders based on alkali-activated metallurgical slags," in *Sustainable and nonconventional construction materials using inorganic bonded fiber composites* (Cambridge, United Kingdom: Woodhead Publishing), 185–220.

Edwards, P. (2014). Global cement magazine. *Glob. Cem. Top.* 100, 2017–2018.

Hewlett, P., and Liska, M. (2019). *Lea's chemistry of cement and concrete* (Butterworth-Heinemann).

Kambole, C., Paige-Green, P., Kupolati, W. K., Ndambuki, J. M., and Adeboje, A. (2019). Comparison of technical and short-term environmental characteristics of weathered and fresh blast furnace slag aggregates for road base applications in South Africa. *Case Stud. Constr. Mater.* 11, e00239. doi:10.1016/j.cscm.2019.e00239

Kani, E. N., Allahverdi, A., and Provis, J. L. (2012). Efflorescence control in geopolymer binders based on natural pozzolan. *Cem. Concr. Compos.* 34 (1), 25–33. doi:10.1016/j.cemconcomp.2011.07.007

Łach, M., Korniejenko, K., Walter, J., Stefańska, A., and Mikuła, J. (2020). Decreasing of leaching and improvement of geopolymer properties by addition of aluminum calcium cements and titanium oxide. *Materials* 13 (3), 495. doi:10.3390/ma13030495

Liaudat, J., Carol, I., and López, C. M. (2020). Model for alkali-silica reaction expansions in concrete using zero-thickness chemo-mechanical interface elements. *Int. J. Solids Struct.* 207, 145–177. doi:10.1016/j.ijsolstr.2020.09.019

Lindgård, J., Andiç-Çakır, Ö., Fernandes, I., Rønning, T. F., and Thomas, M. D. (2012). Alkali–silica reactions (ASR): literature review on parameters influencing laboratory performance testing. *Cem. Concr. Res.* 42 (2), 223–243. doi:10.1016/j.cemconres.2011.10.004

Longhi, M. A., Zhang, Z., Rodríguez, E. D., Kirchheim, A. P., and Wang, H. (2019). Efflorescence of alkali-activated cements (geopolymers) and the impacts on material structures: a critical analysis. *Front. Mater.* 6, 89. doi:10.3389/fmats.2019.00089

Manjunath, R., and Narasimhan, M. C. (2020). Alkali-activated concrete systems: a state of art. *New Mater. Civ. Eng.*, 459–491. doi:10.1016/b978-0-12-818961-0.00013-2

Mo, B. H., Zhu, H., Cui, X. M., He, Y., and Gong, S. Y. (2014). Effect of curing temperature on geopolymerization of metakaolin-based geopolymers. *Appl. clay Sci.* 99, 144–148. doi:10.1016/j.clay.2014.06.024

Msinjili, N. S., and Schmidt, W. (2014). Rice husk ash as a constituent material for low-cost housing in Africa. *Concr. Trends J. Afr. Cem. Concr. Industry* 17 (4), 44–46.

Nodehi, M., and Taghvaee, V. M. (2022). Alkali-activated materials and geopolymer: a review of common precursors and activators addressing circular economy. *Circular Econ. Sustain.* 2 (1), 165–196. doi:10.1007/s43615-021-00029-w

Ramadhansyah, P. J., Mahyun, A. W., Salwa, M. Z. M., Bakar, B. A., Johari, M. M., and Ibrahim, M. W. (2012). Thermal analysis and pozzolanic index of rice husk ash at different grinding time. *Procedia Eng.* 50 (50), 101–109. doi:10.1016/j.proeng.2012.10.013

Saludung, A., Azeyanagi, T., Ogawa, Y., and Kawai, K. (2021). Effect of silica fume on efflorescence formation and alkali leaching of alkali-activated slag. *J. Clean. Prod.* 315, 128210. doi:10.1016/j.jclepro.2021.128210

Scherer, G. W. (2004). Stress from crystallization of salt. *Cem. Concr. Res.* 34 (9), 1613–1624. doi:10.1016/j.cemconres.2003.12.034

Shen, Y., Zhao, P., and Shao, Q. (2014). Porous silica and carbon derived materials from rice husk pyrolysis char. *Microporous Mesoporous Mater.* 188, 46–76. doi:10.1016/j.micromeso.2014.01.005

Shi, C., Roy, D., and Krivenko, P. (2003). *Alkali-activated cements and concretes*. Boca Raton, United States: CRC Press.

Singh, B. (2018). "Rice husk ash," in *Waste and supplementary cementitious materials in concrete* (Cambridge, United Kingdom: Woodhead Publishing), 417–460.

Sithole, T., and Mareya, M. (2023). Turning fly ash and waste gypsum into a resource for backfilling applications. *Case Stud. Constr. Mater.*, e02703.

Škvára, F., Kopecký, L., Myšková, L., Šmilauer, V., Alberovská, L., and Vinšová, L. (2009). Aluminosilicate polymers–influence of elevated temperatures, efflorescence. *Ceramics–Silikáty* 53 (4), 276–282.

Srinivasamurthy, L., Chevali, V. S., Zhang, Z., and Wang, H. (2021). Phase changes under efflorescence in alkali activated materials with mixed activators. *Constr. Build. Mater.* 283, 122678. doi:10.1016/j.conbuildmat.2021.122678

Sun, K., Peng, X., Wang, S., Zeng, L., Ran, P., and Ji, G. (2020). Effect of nano-SiO2 on the efflorescence of an alkali-activated metakaolin mortar. *Constr. Build. Mater.* 253, 118952. doi:10.1016/j.conbuildmat.2020.118952

Wang, L., Chen, M. L., and Tsang, D. C. (2020). "Green remediation by using low-carbon cement-based stabilization/solidification approaches," in *Sustainable remediation of contaminated soil and groundwater* (Butterworth-Heinemann), 93–118.

Yoon, S. J., Son, Y. I., Kim, Y. K., and Lee, J. G. (2012). Gasification and power generation characteristics of rice husk and rice husk pellet using a downdraft fixed-bed gasifier. *Renew. Energy* 42, 163–167. doi:10.1016/j.renene.2011.08.028

Zhang, Z., Provis, J. L., Ma, X., Reid, A., and Wang, H. (2018). Efflorescence and subflorescence induced microstructural and mechanical evolution in fly ash-based geopolymers. *Cem. Concr. Compos.* 92, 165–177. doi:10.1016/j.cemconcomp.2018.06.010

Zhang, Z., Provis, J. L., Reid, A., and Wang, H. (2014). Fly ash-based geopolymers: the relationship between composition, pore structure and efflorescence. *Cem. Concr. Res.* 64, 30–41. doi:10.1016/j.cemconres.2014.06.004

Zhu, Y., Longhi, M. A., Wang, A., Hou, D., Wang, H., and Zhang, Z. (2022). Alkali leaching features of 3-year-old alkali activated fly ash-slag-silica fume: for a better understanding of stability. *Compos. Part B Eng.* 230, 109469. doi:10.1016/j.compositesb.2021.109469